15th Australasian Fluid Mechanics Conference
The University of Sydney, Sydney, Australia
13-17 December 2004

Comparing RANS Models for Flow and Thermal Analysis of Pin Fin Heat Sinks

B. Moshfegh[1] and Robert Nyiredy[2]
[1]Division of Energy Systems, Department of Mechanical Engineering, Linköping University, S-581 83 Linköping, Sweden
[2]Fluent Sweden AB, S-416 64 Göteborg, Sweden

Abstract

The paper discusses various levels of numerical modelling of turbulent flow that are relevant to electronic cooling. Five well-known turbulence models are investigated, i.e., four different eddy-viscosity models; the standard *k-ε*, RNG, the realizable and the *k-ω*, as well as the Reynolds stress model, RSM. Different near-wall treatments have been employed. The accuracy of the numerical schemes has been discussed. The model under consideration is a 3-D model of circular pin fin heat sinks in bypass flow conditions. The experimental data presented by Jonsson and Moshfegh [1] has been used for comparison. Three different inlet velocities have been considered corresponding to a channel *Re* = 5000 to 14500. Results are presented for the base plate temperature, the pressure drop, as well as the influence of flow bypass, and the leakage from the interfin region to the bypass regions of the domain. The result shows that choosing the right turbulence model and near-wall treatments have a great influence on the heat transfer coefficient and the pressure drop.

Introduction

The current trends towards miniaturization, greater functionality and faster processors are resulting in a steady increase in the amount of heat dissipated per unit surface area or unit volume of the electronic components. Usually extended surfaces are used to increase the heat dissipation from electronic components to the ambient air and have been the topic of many studies in recent years. One of the most common types of extended surfaces is the pin fin heat sink. The main advantage of this type of heat sinks is independent of the direction of the incoming flow and it is suitable for the situations where the flow paths are hard to predict. Traditionally, the research in the field of electronic cooling has been dominated by experiments. The performance of pin fin heat sinks in forced convection has been studied quite extensively. Recently a comprehensive experimental investigation, which considered pin fins of different cross shapes, sizes and bypass conditions, was carried out by Jonsson and Moshfegh [1]. Jonsson [2] has also presented a comprehensive literature survey. However, interest has now also turned to numerical investigations, mostly due to the increasing capability of performing CFD simulations. CFD predictions of pin fin heat sinks in forced convection are still quite rare. Yokono and Hisano [3] and Behnia et al. [4] performed CFD analysis on pin fin heat sinks without a flow bypass. Nowadays, thermal management engineers in electronic industries use CFD as a design tool to predict the details of flow and heat transfer. During the past decades, too many turbulence models have been developed and introduced into the market. Thus, it is a rather challenging task to choose the right turbulence model for a specific application. The objective of this study is to investigate the performance of five well-known turbulence models to predict the air flow and heat transfer for pin fin heat sinks under bypass flow conditions. The employed models are four eddy-viscosity models, i.e., the standard *k-ε*, the RNG, the Realizable and the *k-ω*, and the RSM. A steady-state 3-D model is used for simulating the flow and the heat transfer of the pin fin heat sinks under bypass conditions, see Figure 1. The experimental data presented by Jonsson and Moshfegh [1] is used for comparison. It is shown that choosing the right turbulence model and near-wall treatments have a great influence on the heat transfer coefficient and the pressure drop.

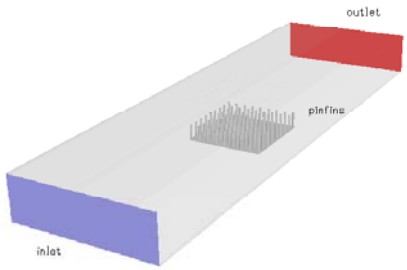

Figure 1. Pin fin heat sink in bypass flow conditions.

Mathematical Modelling

This part of the paper presents the turbulence models used for analysing the flow and heat transfer in a package of circular pin fins under bypass flow conditions. The buoyancy effect is assumed to be negligible and the radiation heat transfer is not included. Based on the above assumptions for steady state, three-dimensional, incompressible turbulent flow the continuity, time-averaged Navier-Stokes and energy equations are given by

$$\frac{\partial U_i}{\partial x_i} = 0 \qquad (1)$$

$$\frac{\partial \left(U_j U_i\right)}{\partial x_j} = -\frac{\partial \overline{P}}{\partial x_i} + \nu \nabla^2 U_i + \frac{\partial}{\partial x_j}\left(-\overline{u_i' u_j'}\right) \qquad (2)$$

$$\frac{\partial \left(U_j T\right)}{\partial x_j} = \alpha \nabla^2 T + \frac{\partial}{\partial x_j}\left(-\overline{u_i' \theta}\right) \qquad (3)$$

where $\overline{P}$ is the modified kinematic pressure and the unknowns, $\overline{u_i' u_j'}$, $\overline{u_i' \theta}$ constitute the *second-moments* statistical correlation or so-called Reynolds stresses and turbulent heat fluxes. These unknowns must be modelled to close the system of equations. The most popular models to approximate these terms are the eddy-viscosity turbulence models and RSM.

The Eddy Viscosity Turbulence Hypothesis

The aim is to analogise the turbulent transport phenomenon to viscous transport and to introduce an *eddy-viscosity* for turbulence by the Boussinesq assumption. Boussinesq eddy-viscosity assumption for $\overline{u_i' u_j'}$, $\overline{u_i' \theta}$ are given by

$$\overline{u_i' u_j'} = -2\nu_t S_{ij} + \frac{2}{3}\delta_{ij} k \,,\quad \overline{u_i' \theta} = -\frac{\nu_t}{\sigma_t}\frac{\partial T}{\partial x_j} \qquad (4)$$

where ν_t is the eddy viscosity, σ_t is the turbulent *Pr* number, *k* is turbulent kinetic energy and $S_{ij} = 0.5(\partial U_i / \partial x_j + \partial U_j / \partial x_i)$.

Two-equation model

This model implies that the length and velocity scales of the mean flow and of the turbulence are proportional and can be related by means of dimensional reasoning to turbulent kinetic, *k*, energy and its dissipation rate, *ε*, $u=k^{0.5}$, $l=k^{1.5}\varepsilon^{-1}$. Considering the above assumption, the turbulent eddy viscosity can be derived as, $\nu_t=C_\mu k^2 \varepsilon^{-1}$, and it is valid only when local isotropy in the turbulence field is assumed. ε is given by

$$\varepsilon = \nu \overline{\frac{\partial u_i'}{\partial x_j}\frac{\partial u_i'}{\partial x_j}} \qquad (5)$$

Thus two-equation eddy-viscosity models require two additional transport equations for k and ε to solve the spatial and temporal variation of the local velocity scale and the length scale.

The Standard k-ε Model

The following transport equations for k and ε are obtained from Reynolds stress transport equation and a model version of the exact transport equation derived from the second moment

$$\frac{\partial(U_j k)}{\partial x_j} = \nu\nabla^2 k - \frac{\partial}{\partial x_j}\left(\frac{1}{2}\overline{u_i' u_i' u_j'} + \frac{\overline{p' u_j'}}{\rho}\right) - \overline{u_i' u_j'}\frac{\partial U_i}{\partial x_j} - \varepsilon \quad (6)$$

$$\frac{\partial(U_j \varepsilon)}{\partial x_j} = \nu\nabla^2 \varepsilon - \nu\frac{\partial}{\partial x_k}\left(\overline{u_k' \frac{\partial u_i'}{\partial x_m}\frac{\partial u_i'}{\partial x_m}} + \overline{\frac{2}{\rho}\frac{\partial p'}{\partial x_m}\frac{\partial u_k'}{\partial x_m}}\right)$$
$$- 2\nu\left(\overline{\frac{\partial u_j'}{\partial x_i}\frac{\partial u_j'}{\partial x_k}} + \overline{\frac{\partial u_i'}{\partial x_j}\frac{\partial u_k'}{\partial x_j}}\right)\frac{\partial U_i}{\partial x_k} - 2\nu\overline{u_k'\frac{\partial u_i'}{\partial x_j}}\frac{\partial^2 U_i}{\partial x_k \partial x_j} \quad (7)$$
$$- 2\nu\overline{\frac{\partial u_i'}{\partial x_k}\frac{\partial u_i'}{\partial x_m}\frac{\partial u_k'}{\partial x_m}} - 2\nu^2\overline{\frac{\partial^2 u_i'}{\partial x^2{}_{km}}\frac{\partial^2 u_i'}{\partial x^2{}_{km}}}$$

These equations are accurate for turbulent kinetic energy and turbulent dissipation rate. Quantities such as Reynolds stresses are still unknown and have to be modelled. The equations of k and ε after approximation are modelled in the high Re models as

$$\frac{\partial(U_j k)}{\partial x_j} = \left(\nu + \frac{\nu_t}{\sigma_k}\right)\nabla^2 k + \nu_t S^2 - \varepsilon \quad (8)$$

$$\frac{\partial(U_j \varepsilon)}{\partial x_j} = \left(\nu + \frac{\nu_t}{\sigma_\varepsilon}\right)\nabla^2 \varepsilon + C_{\varepsilon 1}\frac{\varepsilon}{k}\nu_t S^2 - C_{\varepsilon 2}\frac{\varepsilon^2}{k} \quad (9)$$

where C_μ = 0.09, $C_{\varepsilon 1}$ = 1.44, $C_{\varepsilon 2}$ = 1.92, σ_κ = 1.0, σ_ε = 1.3 and $S = (2S_{ij}S_{ij})^{0.5}$. The k-ε model (hereafter called k-ε) is the most popular of the two-equation eddy viscosity models, but various others have been developed.

The RNG k-ε Model

The coefficients of the k-ε are determined from a number of case studies of simple turbulent flows. Thus the k-ε has a limited board of applicability, which yields poor performance for cases with complex flows. This poor performance is suspected to be due to inaccuracies in the ε-equation. The Renormalization Group k-ε model (RNG) introduces an additional term in the ε-equation, which improves the performance of it. The basic idea is to systematically filter out the small-scale turbulence to a degree that the remaining scales can be resolved. This is done by the parameter, η, which is the ratio between the time scales of the turbulence and the mean flow. The ε-equation is given by

$$\frac{\partial(U_j \varepsilon)}{\partial x_j} = \left(\nu + \frac{\nu_t}{\sigma_\varepsilon}\right)\nabla^2 \varepsilon + C_{\varepsilon 1}\frac{\varepsilon}{k}\nu_t - C^*{}_{\varepsilon 2}\frac{\varepsilon^2}{k} \quad (10)$$

where $\eta = Sk/\varepsilon$, η_0 =4.38, β=0.012, C_μ = 0.0845, $C_{\varepsilon 1}$ = 1.42, $C_{\varepsilon 2}$ = 1.68, $\sigma_\kappa = \sigma_\varepsilon$ = 0.7178 and $C^*{}_{\varepsilon 2} = C_{\varepsilon 2} + \dfrac{C_\mu \eta^3 (1 - \eta/\eta_0)}{1 + \beta\eta^3}$.

The Realizable k-ε Model

"Realizable" means that by numerical clipping, which is introduced in the code, one can remove unphysical values of variables, e.g. negative normal stresses, from the predictions. To achieve the realizability effect the C_μ is no longer constant but a function of the turbulence fields, mean strain and rotation rates. The k equation is identical with Eq. (8) and ε equation is given by

$$\frac{\partial(U_j \varepsilon)}{\partial x_j} = \left(\nu + \frac{\nu_t}{\sigma_\varepsilon}\right)\nabla^2 \varepsilon + C_1 S\varepsilon - C_2\frac{\varepsilon^2}{k + \sqrt{\nu\varepsilon}} \quad (11)$$

where C_1 = max [0.43, $\eta/(\eta$+5)], C_2 = 1.0, σ_κ = 1.0, σ_ε = 1.2.

The k-ω Model

The standard k-ω model with low Re effects has been used. The k-ω model is based on model transport for the turbulent kinetic energy, k, and the specific dissipation rate, $\omega = \varepsilon/k$. The ω equation is defined as

$$\frac{\partial(U_j \omega)}{\partial x_j} = \left(\nu + \frac{\nu_t}{\sigma_\omega}\right)\nabla^2 \omega + C_{\omega 1}\frac{\omega}{k}\nu_t S^2 - C_{\omega 2}\omega^2 \quad (12)$$

Reynolds Stress-Transport Model, RSM

The RSM is one of the most sophisticated tools currently used by engineers to predict turbulent flows with complex strain fields or significant body forces. RSM or a so-called second-moment model is based on modelled versions of the exact but intractable Reynolds stress transport equations. The aim is to solve the unknowns introduced when averaging Navier-Stokes equations. For non-isothermal 3-D turbulent flows, it is necessary to solve nine full partial differential transport equations for six unknown Reynolds stresses and three turbulent heat fluxes and one equation for transport of ε. k is found by adding the three normal stresses. Equation for the transport of $R_{ij} = \overline{u_i' u_j'}$ is given by:

$$\frac{\partial(U_j R_{ij})}{\partial x_j} = \left(\nu + \frac{\nu_t}{\sigma_k}\right)\nabla^2 R_{ij} - R_{ik}\frac{\partial U_j}{\partial x_k} - R_{jk}\frac{\partial U_i}{\partial x_k}$$
$$- \frac{2}{3}\delta_{ij}\varepsilon - \overline{\frac{p'}{\rho}\left(\frac{\partial u_i'}{\partial x_j} + \frac{\partial u_j'}{\partial x_i}\right)} \quad (13)$$

where the terms on the right side of the equation are the molecular and turbulent diffusion (after modelling), stress production (no need for modelling), dissipation (after modelling) and pressure strain. Linear pressure strain model is used to model the pressure strain term in this study. The ε equation is given by:

$$\frac{\partial(U_j \varepsilon)}{\partial x_k} = \left(\nu + \frac{\nu_t}{\sigma_\varepsilon}\right)\nabla^2 \varepsilon - C_{\varepsilon 1} R_{ij}\frac{\partial U_i}{\partial x_j}\frac{\varepsilon}{k} - C_{\varepsilon 2}\frac{\varepsilon^2}{k} \quad (14)$$

where C_μ = 0.09, $C_{\varepsilon 1}$ = 1.44, $C_{\varepsilon 2}$ = 1.92, σ_κ = 0.82, σ_ε = 1.0.

Near-Wall Treatments

For high Re models (i.e. k-ε, RNG, Realizable and RSM), three different near-wall treatment options have been used in the present investigation that is the Standard wall function (SW) proposed by Launder and Spalding, the Enhanced wall function (EW) and the Non-equilibrium wall approach (NW). The SW is well known and will not be discussed here. The EW subdivides the near wall region into a viscous sub-layer and a fully turbulent flow. In the viscous sub-layer region, only the k equation is solved, while in the fully turbulent flow the k-ε or RSM is computed. The term wall distance is introduced to compute the interface between the two layers. The idea behind the non-equilibrium wall function not only considers the equilibrium assumption (production=dissipation) for computing the budget for the kinetic energy adopted by the SW, but also takes into account the budget of kinetic energy, which can vary widely in highly non-equilibrium flows involving strong pressure gradients. This effect can be implemented by introducing the pressure gradient term in the log law in order to sensitise the mean velocity. For the k-ω, the near wall approach will be employed. This means that the near-wall region will be completely resolved all the way down to the viscous sub-layer.

Geometry and boundary conditions

The problem domain consists of a heated base plate with circular pin fin heat sinks placed on the floor of a rectangular channel. A sketch of the set-up is shown in Figure 1. The x, y and z directions are in stream-wise, normal and span-wise directions, respectively. The channel dimensions are, length by width by

height, 350×100×30 mm. The base plate has the following dimensions, length by width by thickness, 52.8×52.8×3 mm. Only one pin fin heat sink configuration is modelled with the following dimensions, a pin diameter of 1.5 mm and a fin-to-fin distance of 4.9 mm. The selected heat sink is an inline 9×9 circular pin fin heat sink with a fin height of 10 mm. The distance from the inlet to the leading edge of the heat sink is 150 mm and the distance from the trailing edge of the heat sink to the domain outlet, is 147.2 mm. For validation of the numerical model, three experimental cases, see Jonsson and Moshfegh [1] have been used. The simulations were conducted under the same boundary conditions as the experiments were performed, see Table 1.

	Case 1	*Case 2*	*Case 3*
U_{in}, [m/s]	1.57	3.00	4.59
T_{in}, [˚C]	17.5	17.5	17.5
q_{in}, [W]	9.19	9.42	9.52
$q"_{in}$, [W/m^2]	3298	3342	3411

Table 1. Set-up boundary conditions for the numerical model.

The inlet turbulence intensity is assumed to be 5%. The simulations were performed for the following *Re*, $Re_d = \rho U_{in} d_h/\mu$, 5000, 9500 and 14500, based on the channel hydraulic diameter, d_h. The physical properties of air and aluminium are summarised in Table 2 and are constant during the simulation.

	Air	*Aluminium*
λ, [W/m K]	0.0242	202.4
μ, [kg/m s]	$1.789 \cdot 10^{-5}$	-
ρ, [kg/m^3]	1.225	2719
C_p, [J/kg K]	1006.43	871

Table 2. Physical properties of air and aluminium.

For a detail discussion about the experimental errors see Jonsson [2]. The resulting maximum relative errors for the cases 1-3 vary between 4.6 to 37.6% and 3.0 to 3.6% for T_b and Δp respectively.

Computational Grids

The Gambit [5] grid generation package is used to generate the 3-D unstructured grid. Due to symmetry conditions in the span-wise direction, only half of the channel is considered. Two grids of different density are used for computation of the test cases. The coarse grid has 360 333 hexahedral cells. The mesh close to the pins is finer with a mesh distribution of 108×52×35. The mesh is non-conformal at the interface between fine and coarse region. The grid distribution for the coarse mesh has been effectively controlled by clustering the mesh towards the walls and edges in such a way that the wall function can be applied properly, i.e. the first numerical point was always located at y^+>15. The finer grid ensured that the wall nearest y^+ is kept close to one near the walls and edges. The finer grid consists of 1 710 027 cells and is used for computation with the *k-ω*. Figure 2 zooms up the coarse and fine computational grids.

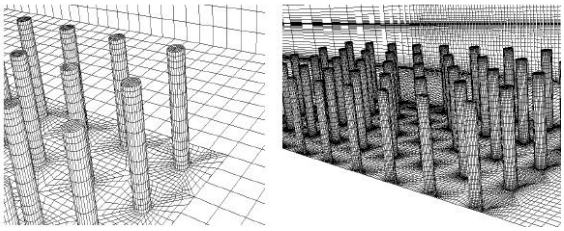

Figure 2. Non-conformal (left) and conformal (right) grid structures are used for coarse and fine mesh respectively.

Numerical Accuracy

FLUENT 6.0 [6] is used to numerically simulate the airflow and thermal behaviour of the heat sinks under bypass flow conditions. The governing equations are solved with a segregated scheme. The governing equations are discretized spatially with first and second order upwind as well as with the Quick schemes for checking the dependency of the results on a scheme level. The SIMPLE algorithm solves the pressure-velocity coupling. The following under relaxation factors are used for the *p*, *U*, *k*, ε and *T*, 0.3, 0.7, 0.8, 0.8 and 1.0. With the fine grid, it takes about 8 hours CPU-time on a 1.4 GHz Pentium-4 to get the result.

Results

Effect of the near-wall treatments on the base plate temperature and pressure drop

Table 3 illustrates the influence of the near-wall treatments on different *k-ε* models. All turbulence models with Standard and Enhanced wall functions over-predict both the mean base plate temperature, T_b, and the pressure drop, Δp. Generally, both the *k-ε* and RNG yield similar results with a small advantage for the RNG compared with the measured case. The SW provides the best agreement with the experimental measurement. The non-equilibrium wall treatments over-predict the Δp and under-predict the T_b, which indicates poor agreement with the measured case.

	Case 2	*k-ε*			*RNG*			*Realizable*		
		SW	EW	NW	SW	EW	NW	SW	EW	NW
T_b, [˚C]	35.8	38.8	39.6	34.6	38.6	39.4	34.4	39.7	39.7	34.9
CFD/Exp	-	8.3	10.5	-3.4	7.7	9.8	-4.0	10.7	10.7	-2.7
Δp	2.38	2.70	2.69	3.65	2.61	2.67	3.26	2.58	2.71	3.89
CFD/Exp	-	13.3	13.2	53.4	9.6	12.1	37.1	8.4	13.9	63.6

Table 3. The effect of the near-wall treatments on T_b and Δp.

Effect of the discretization schemes on the base plate temperature and pressure drop

Table 4 shows that the second order upwind discretization provides a significant improvement on the magnitude of the Δp compared to the first order upwind scheme. However, the lower pressure drop will raise the base plate temperature according to Reynolds analogy. In general, the second order upwind is recommended for complex flows such as those presented in this study. As it is shown in Table 4, the Quick discretization did not influence the magnitude of the pressure drop and only reduced the mean base plate temperature with 0.3˚C. Thus the accuracy of the second order scheme is quite acceptable for the present study.

	Case 2	*First order*	*Second order*	*Quick*
T_b, [˚C]	35.8	37.9	39.4	39.1
CFD/Exp	-	5.7%	9.8%	9.0%
Δp, [N/m^2]	2.38	3.18	2.67	2.67
CFD/Exp	-	33.7%	12.0%	12.0%

Table 4. The effect of the discretization schemes on T_b and Δp.

Comparing all turbulence models for Case two

Table 5 compares the predictions obtained by different turbulence models with the experimental data for the T_b and the Δp for Case two. EW treatments have been used as near-wall approach for high *Re* models. For the T_b the *k-ω* gives a better prediction while the Δp prediction by RNG shows the best agreement with the experimental one. Surprisingly, the RSM predictions are nearly the same as the employed two-equation models. One possible clue can be the usage of the isotropic eddy-viscosity hypothesis employed in the present study for RSM instead of the non-linear eddy viscosity modelling.

	Case 2	*Coarse mesh*				*Fine mesh*
		k-ε	*RNG*	*Real.*	*RSM*	*k-ω*
T_b, [˚C]	35.8	39.6	39.4	39.7	39.6	38.8
CFD/Exp	-	10.5%	9.8%	10.7%	10.5%	8.2%
Δp, [N/m^2]	2.38	2.69	2.67	2.71	2.69	2.93
CFD/Exp	-	13.2%	12.1%	13.9%	13.2%	22.9%

Table 5. The effect of the turbulence modelling on T_b and Δp.

Comparing Case 1-3 with RNG, RSM and *k-ω*

Table 6 compares the experimental results for three different inlet velocities with the numerical one. As it is shown, better agreement has been obtained between the CFD predictions and experimental data by increasing the channel *Re*. The RNG shows better overall agreement compared to the other models.

		Exp	*RNG*	*RSM*	*k-ω*
Case 1	T_b, [˚C]	44.9	50.2	50.1	49.5
	CFD/Exp	-	11.9%	11.8%	10.3%
	Δp, [N/m^2]	0.71	0.77	0.85	0.91
	CFD/Exp	-	7.9%	19.3%	28.4%
Case 2	T_b	35.8	39.4	39.5	38.8
	CFD/Exp	-	9.8%	10.3	8.2%
	Δp	2.38	2.67	2.7	2.93
	CFD/Exp	-	12.1%	14.5	22.9%
Case 3	T_b	31.9	34.5	34.6	33.8
	CFD/Exp	-	8.0%	8.2%	5.8%
	Δp	5.72	6.07	6.05	6.40
	CFD/Exp	-	6.0%	5.8%	12.0%

Table 6. Comparison between the CFD and experimental data.

Effect of the inlet velocity on the frontal bypass ratio, tip and side leakage

Table 7 illustrates the influence of the inlet velocity on the frontal bypass ratio, the tip and side leakage, respectively; for more information about the definition of the bypass ratio and leakage, see Jonsson and Moshfegh [1]. As can be seen in the table below, the frontal bypass ratio decreases by increasing the inlet velocity, which means that more air is passing through the heat sink package. About 37% of the flow entering the heat sink leaks from the tip to the bypass area and is nearly constant for the three simulated cases. The side leakage also varies with the inlet velocity. An increase of the inlet velocity will increase the side leakage. At the lowest inlet velocity, almost 8.5% of the flow entering the heat sink leaks out from the side.

	Bypass Ratio	*Tip Leakage*	*Side Leakage*
Case 1	24.3%	37.2%	8.5%
Case 2	22.4%	37.7%	10.9%
Case 3	21.4%	37.5%	12.9%

Table 7. The effect of inlet velocity on the frontal bypass ratio, tip and side leakage for all three cases.

Figure 3 shows the flow and temperature behaviour of the air entering the heat sink and the side and tip leakage predicted by RNG for Case two. A wave motion has been observed at the top of the heat sink, which is damped in the stream-wise direction. Most of the turbulent kinetic energy is produced along the first rows in the stream-wise direction. The air-flow pattern at the side of the heat sinks also shows sinusoidal motion. A small re-circulation cell has also been observed between the pins close to the base plate in the stream-wise direction. The surface temperature of the pins and the air temperature increase in the stream-wise direction.

Figure 4 shows the pressure and velocity as well as the temperature contours in *xz* plane at y = 5 mm predicted by RNG for Case two. Larger pressure drop are observed at the first rows in the stream-wise direction. The contour of the pressure field shows also multiple contractions and expansions as well as redevelopment of the boundary layers in the stream-wise direction causing higher pressure drop compared to the other heat sinks such as plate fin heat sink. In some region, the magnitude of the velocity in the bypass region is higher than the inlet velocity. The penetration of the hot air from interfin to the side bypass is clearly presented in Figure 4.

Conclusions

Four eddy viscosity models and Reynolds stress model are used to predict the airflow and heat transfer in a pin heat sink configuration under bypass flow conditions. The RNG performed the best agreement with the experimental data. The validation of the numerical results has been limited to the static pressure drop before and after the heat sinks and average base plate temperature. Nevertheless, the differences are considerable in some cases, especially at the lower upwind level. It should be noted that more detailed experimental data are necessary for a comprehensive validation analysis. The non-equilibrium wall approach indicates poor agreement with the measured case, while the Standard wall function and Enhanced wall functions provide good agreement with the experimental measurement. Numerical predictions show that about 37% of the flow entering the heat sink leaks from the tip to the bypass area and is nearly constant for the three simulated cases. The side leakage is about 8.5% of the flow entering the heat sink at the lowest velocity and increases by increasing the inlet velocities.

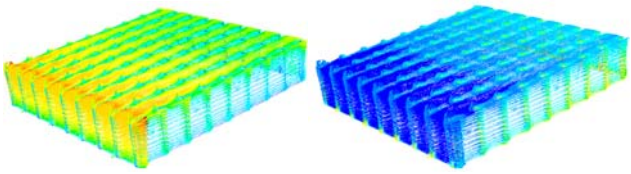

Figure 3. The velocity vector coloured with velocity (left) and temperature (right) values for the bypass domain.

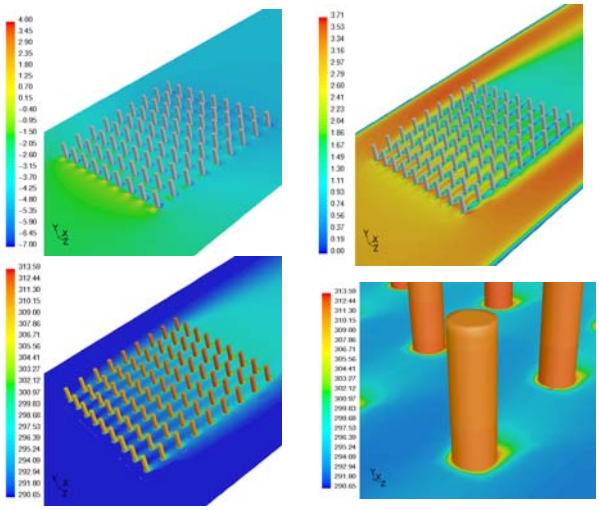

Figure 4. The pressure, velocity and temperature field predicted at y = 5 mm through by RNG for Case two.

References

[1] Jonsson, H. and Moshfegh, B., CFD Modeling of the Cooling Performance of Pin Fin Heat Sinks Under Bypass Flow Conditions, *Proceedings of the InterPACK 2001*, Kauai, Hawaii, USA, 2001.

[2] Jonsson, H., *Turbulent Forced Convection Air Cooling of Electronics with Heat Sinks Under Flow Bypass Conditions*, Doctoral Thesis, Royal Institute of Technology, Department of Energy Technology, Stockholm, Sweden, ISSN 1102-0245, ISRN KTH/REFR/R-01/28-SE, 2001.

[3] Yokono, Y., Hisano, K., Numerical Simulation for Thermal Resistance of Finned LSI Packages, *Advances in Electronic Packaging*, **EEP-Vol. 4-2**, ASME, 1973.

[4] Behnia, M., Copeland, D., Soodphakdee, D., A Comparison of Heat Sink Geometries for Laminar Forced Convection: Numerical Simulation of Periodically Developed Flow, *Proc. 6th InterSociety Conf. on Thermal and Thermomechanical Phenomena in Electronic Systems (ITherm 1998)*, IEEE, 310-315, ISBN 0-7803-4475-8, 1998.

[5] Gambit 2.0, *Gambit Manuals*, Fluent Inc. December 2001.

[6] Fluent 6.0, *Fluent Manuals*, Fluent Inc, December 2001.